Coulomb Barrier for Charge Separation at an Organic Semiconductor Interface

Matthias Muntwiler,* Qingxin Yang, William A. Tisdale, and X.-Y. Zhu+

University of Minnesota, Department of Chemistry, 207 Pleasant St SE, Minneapolis, Minnesota 55455, USA

(Received 1 May 2008; revised manuscript received 2 October 2008; published 6 November 2008)

Charge transfer (CT) excitons across donor-acceptor interfaces are believed to be barriers to charge separation in organic solar cells, but little is known about their physical characteristics. Here, we probe CT excitons on a crystalline pentacene surface using time-resolved two-photon photoemission spectroscopy. CT excitons of 1*s*, 2*s*, and 3*s* characters are bound by Coulomb energies of 0.43, 0.21, 0.12 eV, respectively, in agreement with quantum mechanical modeling. The large binding energy of the 1*s* CT exciton excludes its participation in photovoltaics. Efficient charge separation in organic heterojunction solar cells must involve a series of hot CT excitons.

DOI: 10.1103/PhysRevLett.101.196403 PACS numbers: 71.35.−y, 72.40.+w, 73.20.−r, 73.61.Ph

Photon absorption by a small molecule or polymer in an organic photovoltaic cell creates a singlet exciton, with an estimated binding energy of ≈0.5–1.0 eV [1]. The singlet exciton can only dissociate by a large applied electric field [1,2] or at an interface with another organic semiconductor, i.e., the donor-acceptor (D/A) interface [3,4]. In the latter, dissociation occurs if the energetic driving force, i.e., the offset in the lowest unoccupied molecular orbitals (LUMOs) or the highest occupied molecular orbitals (HOMOs) at the D/A interface, is sufficient to overcome the exciton binding energy. Because of the low dielectric constant of organic materials, Coulomb attraction between the electron and the hole is sufficiently long ranged and singlet exciton dissociation at the D/A interface does not result in free carriers (polarons) but rather a bound electron-hole pair or charge transfer (CT) exciton [Fig. 1(a)] [2,5–7]. The CT exciton is also referred to as an exciplex for the lowest energy CT state or a geminate pair for higher energy levels. Red-shifted fluorescence from exciplexes has been observed in a number of donor-acceptor systems, and other CT states or geminate pairs have been suggested as intermediates for charge carrier separation [5–7]. From a mechanistic perspective, how a CT exciton participates in charge separation depends critically on its binding energy, as well as the spatial extent and symmetry of its wave function.

Here, we probe the CT exciton on the surface of an organic semiconductor using femtosecond time-resolved two-photon photoelectron spectroscopy (TR-2PPE) [8,9]. In this approach, a first photon $h\nu_1$ excites an electron from the HOMO to above the organic semiconductor surface [Fig. 1(b) and 1(c)]. The excited electron is transiently bound by the Coulomb potential from the hole as well as polarization of the organic semiconductor; the latter contribution gives rise to an image-potential state (IPS) which is well understood on polarizable surfaces [8,10]. After a certain time delay, a second photon $h\nu_2$ ionizes the electron for detection. Note that the IPS in Fig. 1(b) is not important to the organic D/A interface in Fig. 1(a), but the electron-hole attraction potential and the resulting CT excitons are similar in both cases. We choose pentacene for the organic semiconductor because it is perhaps the most extensively characterized model organic semiconductor and has been demonstrated to be an efficient electron donor in OPVs [11]. Furthermore, high-quality thin films with bulklike structure can be prepared epitaxially on a Bi(111) substrate from vapor deposition in ultrahigh vacuum [12]. Details about sample preparation and characterization, as well as the experimental setup, are given in the online supporting material [13].

For the 2PPE experiments, the third harmonic (≈0.1 nJ per pulse) and the fundamental (≈1 nJ per pulse) output of a femtosecond Ti:sapphire oscillator (pulse width ≈80 fs) are used as pump and probe pulses, respectively, and photoelectrons are detected by a hemispherical electron energy analyzer [13]. Figure 2(a) shows 2PPE spectra for pentacene film thicknesses of 1–4 ML measured at $h\nu_1 = 4.16$ eV and $h\nu_2 = 1.39$ eV. The energy scale is referenced to the Fermi level (work function = 3.94 eV). The spectrum for 1 ML pentacene shows two distinct peaks due to the transient population of two unoccupied states at energies of 2.99 and 3.42 eV. These states are assigned to a CT exciton (1*s*) and the $n = 1$ image-potential state (IPS) on pentacene, respectively. Supporting this assignment, we find the electron densities $|\psi|^2$ of both states are concentrated in the vacuum above the surface. This is established experimentally by physisorbing a layer of molecular dielectric, *n*-nonane (C_9H_{20}), onto the 1 ML pentacene/Bi surface [13]. As shown in Fig. 2(b), the two peaks are completely quenched as these states are heavily perturbed by the adlayer. Upon desorption of nonane, the original spectrum is recovered. Further support for the assignment comes from dispersion measurements and quantum mechanical modeling, as detailed below. Note that the peak at the low-kinetic threshold (labeled $1h\nu$) in Fig. 2(a) arises due to one-photon photoemission (as verified by the dashed spectrum taken with pump photon only) from occupied Bi states near the Fermi level because $h\nu_1$ is slightly greater

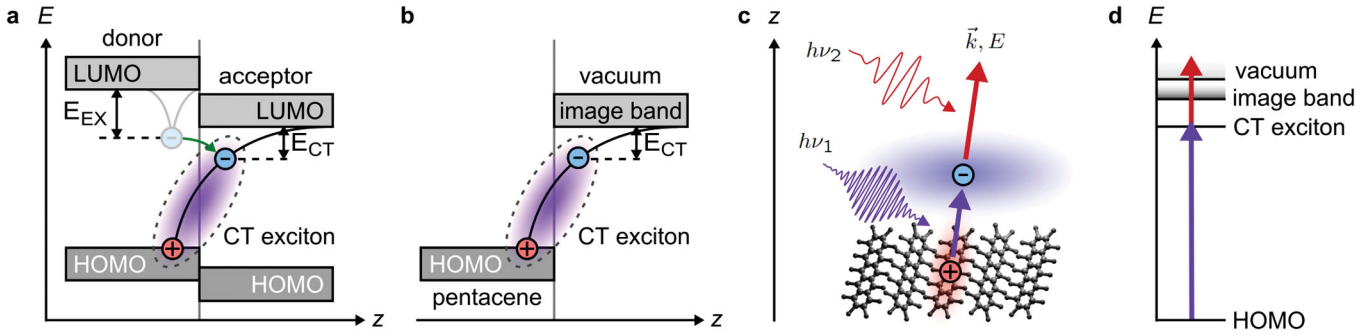

FIG. 1 (color). (a) Dissociation of a singlet exciton to form a charge-transfer exciton (dashed oval) across the donor-acceptor interface. E_{EX} is the singlet exciton binding energy and E_{CT} is the charge-transfer exciton binding energy; (b) CT exciton on the surface of an organic semiconductor with the image band serving as electron acceptor; (c), (d) Sketch of the 2PPE process: A first photon ($h\nu_1$) excites an electron from an occupied molecular orbital into an unoccupied charge-transfer state above the surface. After a time delay, a second photon ($h\nu_2$) ejects the electron to the vacuum where its energy and momentum are analyzed.

than the work function. A spectrum of the clean Bi(111) surface is displayed for comparison in Fig. 2 of the supporting material [13].

With increasing pentacene film thickness, the IPS peak vanishes while the CT_{1s} peak remains and shifts slightly (−0.06 eV) to lower energy. The different coverage dependencies establish that the initial states involved in photoexcitation to the CT exciton and the IPS are different. A recent one-photon photoemission measurement on the same system put the HOMO of pentacene at 1.2 eV below the Fermi level [14]. The initial state of the IPS peak lies in the HOMO-LUMO gap of pentacene and must be located in the Bi substrate. Spatial wave function overlap between the IPS and Bi substrate states becomes negligible for pentacene films thicker than 1 ML, and thus the IPS cannot be populated by photoexcitation. In contrast, the pump photon ($h\nu_1 = 4.16$ eV) is in resonance with the HOMO → CT_{1s} transition, and thus the CT_{1s} state is observed for all pentacene film thicknesses investigated. When we increase the pump photon energy to $h\nu_1 = 4.38$ eV, hot CT excitons with energies higher than the one of the 1s state come into resonance, as shown in Fig. 2(c). The two high energy peaks in the spectrum are located at 0.22 and 0.31 eV above CT_{1s}. Quantum mechanical modeling (see below) shows that these two states correspond to the 2s and 3s CT excitons. Similar hot CT excitons are observed at all pentacene film thicknesses investigated (1–7 ML).

Both the image potential state and the associated CT excitons are short-lived because they are energetically located high above the Fermi level and can decay into unoccupied states (LUMO + N) in the pentacene thin film. Figure 3(a) shows pump-probe cross-correlation measurements on 1 ML pentacene/Bi obtained for the IPS and the CT at peak electron energies. These curves give single exponential decay times of $\tau_{IPS} = (134 \pm 10)$ fs and $\tau_{CT} = (78 \pm 10)$ fs. Within the lifetime of both states, we find no significant shifts in peak positions, i.e., no measurable energy relaxation [Fig. 3(b)].

An important experimental feature which distinguishes the CT exciton from an IPS is dispersion parallel to the surface. An electron in an IPS is bound by the polarization potential in the surface normal direction but is free in the surface plane and thus exhibits free-electron-like dispersion $E = E_0 + (\hbar k_{||})^2/(2m^*)$ parallel to the surface. In contrast, photoemission from an exciton does not show

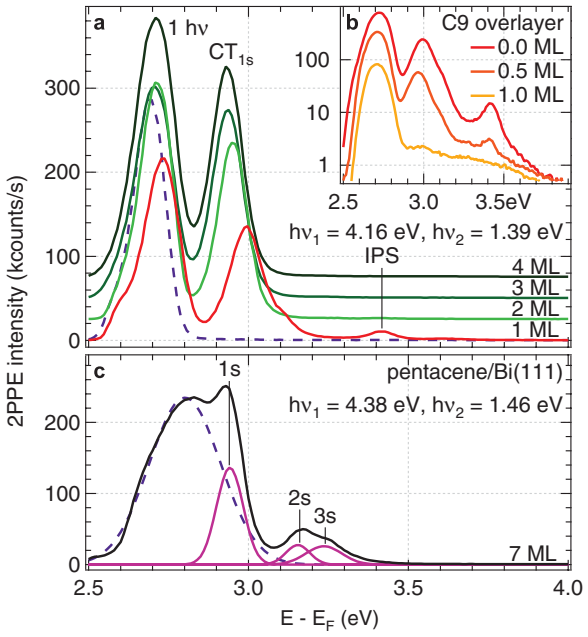

FIG. 2 (color). (a) 2PPE spectra from pentacene/Bi(111) surfaces ($h\nu_1 = 4.16$ eV; $h\nu_2 = 1.39$ eV) in the pentacene film thickness ranges of 1 to 4 monolayer (ML). The dashed spectrum was obtained with $h\nu_1$ only. CT: charge-transfer exciton; IPS: image-potential state. (b) 2PPE spectra from 1 ML pentacene/Bi with 0, 0.5, and 1 ML nonane overlayer. (c) 2PPE spectrum (gray curve) and Gaussian decompositions (dashed curve for one-photon component and pink curves for CT excitons) obtained for 7 ML pentacene at the indicated photon energies ($h\nu_1 = 4.38$ eV; $h\nu_2 = 1.46$ eV).

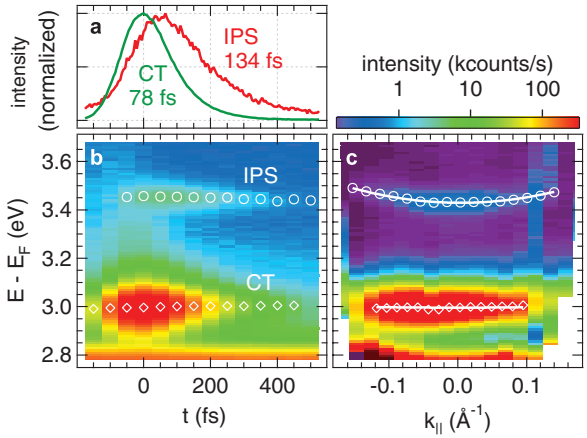

FIG. 3 (color). (a) Cross-correlation curves at the CT_{1s} and IPS energies. Intensities of the two curves have been normalized; (b) Time-resolved 2PPE spectra with UV pump and IR probe pulses. Markers denote peak positions; (c) Pseudocolor representation of momentum-resolved 2PPE spectrum. Markers denote peak positions. The upper image-potential state is well described by free electron-like dispersion (line) with an effective mass of $1.5m_e$, whereas the lower nondispersive CT exciton peak exhibits no dispersion.

dispersion because the photoionization process destroys the quasiparticle [15]. This is verified in Fig. 3(c) which shows a pseudocolor plot of 2PPE spectra taken at different detection angles (i.e., different parallel momentum vectors, $k_{||}$). The IPS clearly shows dispersion with the bottom of the image band at $E_0 = 3.42$ eV and an effective electron mass of $m^\star \approx 1.5m_e$, whereas the CT_{1s} state shows no dispersion. Similarly, no dispersion is found for the CT_{2s} and CT_{3s} states (data not shown).

To quantitatively understand the IPS and the CT exciton, we consider the Coulomb potential within the dielectric continuum approximation. This potential is the sum of two contributions: the image potential

$$V_i = -\frac{e^2}{4\pi\epsilon_0}\frac{\beta}{4z} \tag{1}$$

and attraction by the positive hole

$$V_h = -\frac{e^2}{4\pi\epsilon_0}\frac{\gamma}{\sqrt{x^2 + y^2 + (z - z_h)^2}}, \tag{2}$$

where the z axis corresponds to the surface normal with the image plane at $z = 0$ and the hole at $(0, 0, z_h)$. ϵ_0 is the vacuum permittivity, and e is the electron charge. $\beta = \frac{\epsilon-1}{\epsilon+1}$ and $\gamma = \frac{2}{\epsilon+1}$ account for screening of the charges due to polarizability of pentacene [16] with a relative dielectric constant $\epsilon \approx 5.3$ along the surface normal [17,18].

We solve the three-dimensional Schrödinger equation numerically using the finite element method within the COMSOL simulation software. The solutions can be divided into two regimes: A band of delocalized states which corresponds to the image band, and a series of localized, bound states converging towards the bottom of the image band. As expected, the image band possess free-electron-like dispersion (data not shown). Figure 4(a) shows the energy levels of the localized states with respect to the bottom of the image band for $\epsilon = 5.3$ and $z_h = -2.7$ Å. These states correspond to CT excitons: In addition to the image potential, they are bound by the electron-hole Coulomb potential of Eq. (2). The dependence of the binding energy E_{CT} of the lowest CT exciton on the two parameters ϵ and z_h is plotted in Fig. 4(c). We choose $\epsilon = 5.3$ based on literature value [17], whereas z_h is chosen such that the calculated $E_{CT,1s}$ matches the experimental value of 0.43 eV for the $1s$ state on 1 ML pentacene. The simulation then predicts that the $2s$ and $3s$ CT excitons have binding energies of 0.21 and 0.12 eV, respectively, in excellent agreement with experimental results in Fig. 2. According to the cylindrical symmetry of the potential, the wave functions have discrete angular momentum l_z [Fig. 4(b)]. Within the energetic range probed, the $1p$ state is clearly missing in the experiment [Fig. 2(c)]. This is because the π-HOMO $\rightarrow CT_{1p}$ optical transition is forbidden due to the selection rule on orbital angular momentum.

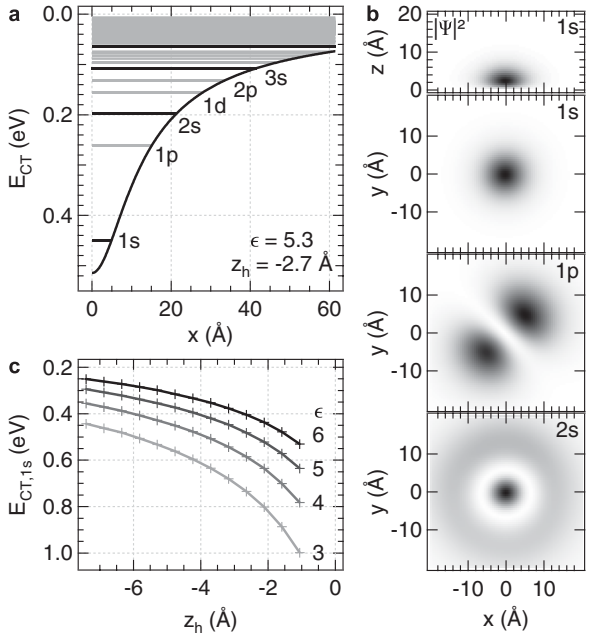

FIG. 4. Finite element solutions of the stationary Schrödinger equation for the model potential, Eqs. (1) and (2). (a) Calculated eigenvalues for $\epsilon = 5.3$ and $z_h = -2.7$ Å. Black and dark gray lines denote localized CT exciton states with angular momentum $l_z = 0$ and $l_z \neq 0$, respectively. The curved line represents the potential at the center of the IPS wave function, 6.2 Å above the image plane. (b) Two-dimensional cuts through the electron densities $|\psi|^2$ of the three lowest states. (c) Calculated binding energies of the CT_{1s} exciton as a function of the hole position z_h and dielectric constant ϵ. The energy scale E_{CT} is referenced to the bottom of the image band.

The transition to $1d$ is allowed but not resolved from $2s$ and $3s$. Given z_h and the resulting expectation value of z, $\langle z \rangle_{1s} = 3.6$ Å, the average electron-hole distance in the lowest CT exciton state amounts to 6.3 Å, which is close to the size of two aromatic rings in a pentacene molecule.

The pentacene-vacuum interface represents a model for donor-acceptor interfaces in organic photovoltaic because the electrostatic potential V_h of the pentacene or vacuum system is equivalent to that of a D/A interface with an average dielectric constant of $\bar{\epsilon} = 1/\gamma = 3.15$, which is typical for materials used in heterojunction OPV cells. Therefore, the $1s$ CT exciton binding energy of 0.43 eV is representative of the Coulomb barrier for charge separation at heterojunctions. This binding energy is more than 1 order of magnitude higher than $k_B T$ at room temperature, and thus, charge separation from the $1s$ CT exciton has a very low probability. For this reason, charge separation in OPV must involve hot CT exciton states: (1) Compared to the $1s$ CT state, hot CT excitons are more weakly bound by the Coulomb potential; (2) density-of-states of these hot excitons increase with energy in the Coulomb potential; and (3) electronic coupling from a singlet exciton in the donor to a hot CT exciton across the D/A interface can be higher than that to a $1s$ CT exciton due to a lower energy denominator [19]. Previous studies on organic D/A blends indeed suggested that charge separation was more efficient for an e-h pair (geminate pair) at longer distance than that of the exciplex [5–7]. This classical picture of a geminate pair is essentially a higher lying CT exciton state shown in Fig. 4. It is well known that efficient charge separation at a D/A interface requires a sufficient energetic driving force, i.e., offset in LUMO or HOMO levels [3,4]. Such excess electronic energy can also be essential in leading to the population of hot CT excitons that undergo efficient charge separation [20]. All these factors point to the essential role of hot CT excitons in charge carrier separation at D/A interfaces in organic heterojunction solar cells.

In conclusion, the presented results give direct experimental evidence for a series of discrete, localized charge-transfer exciton states at the surface of an organic semiconductor, pentacene. Given the general nature of the potentials, i.e., the image potential due to polarizability of the surface and the Coulomb potential due to the photohole, CT excitons must be considered a universal feature of photoexcited organic semiconductor surfaces. These results also suggest a key design principle in organic heterojunction solar cells: there must be strong electronic coupling between singlet excitons in the donor and hot CT excitons across the D/A interface.

The authors would like to thank Y. Xia and C. D. Frisbie for providing purified pentacene, G. E. Thayer and J. T. Sadowski for advice on sample preparation, and the Minnesota Supercomputing Institute for computing time. This work was supported primarily by the MRSEC Program of the National Science Foundation under Grant No. DMR-0212302, in part by the US Department of Energy (DE-FG02-07ER46468), and the National Science Foundation (DMR-0804583). W. A. T. acknowledges financial support from the IGERT program (DGE-0114372).

*muntw001@umn.edu
+Corresponding author: zhu@umn.edu

[1] V. I. Arkhipov and H. Bässler, Phys. Status Solidi A **201**, 1152 (2004).
[2] M. Yokoyama, Y. Endo, A. Matsubara, and F. H. Mikawa, J. Chem. Phys. **75**, 3006 (1981).
[3] B. P. Rand, D. P. Burk, and S. R. Forrest, Phys. Rev. B **75**, 115327 (2007).
[4] M. Scharber, D. Mühlbacher, M. Koppe, P. Denk, C. Waldauf, A. Heeger, and C. Brabec, Adv. Mater. **18**, 789 (2006).
[5] V. D. Mihailetchi, L. J. A. Koster, J. C. Hummelen, and P. W. M. Blom, Phys. Rev. Lett. **93**, 216601 (2004).
[6] P. Peumans and S. R. Forrest, Chem. Phys. Lett. **398**, 27 (2004).
[7] A. C. Morteani, P. Sreearunothai, L. M. Herz, R. H. Friend, and C. Silva, Phys. Rev. Lett. **92**, 247402 (2004).
[8] T. Fauster, C. Reuß, I. L. Shumay, and M. Weinelt, Chem. Phys. **251**, 111 (2000).
[9] C. Gahl, U. Bovensiepen, C. Frischkorn, and M. Wolf, Phys. Rev. Lett. **89**, 107402 (2002).
[10] M. W. Cole and M. H. Cohen, Phys. Rev. Lett. **23**, 1238 (1969).
[11] S. Yoo, B. Domercq, and B. Kippelen, Appl. Phys. Lett. **85**, 5427 (2004).
[12] J. T. Sadowski, T. Nagao, S. Yaginuma, Y. Fujikawa, A. Al-Mahboob, K. Nakajima, T. Sakurai, G. E. Thayer, and R. M. Tromp, Appl. Phys. Lett. **86**, 073109 (2005).
[13] EPAPS Document No. E-PRLTAO-101-084846, for materials containing details on sample preparation and characterization. For more information on EPAPS, see http://www.aip.org/pubservs/epaps.html.
[14] H. Kakuta, T. Hirahara, I. Matsuda, T. Nagao, S. Hasegawa, N. Ueno, and K. Sakamoto, Phys. Rev. Lett. **98**, 247601 (2007).
[15] M. Weinelt, M. Kutschera, T. Fauster, and M. Rohlfing, Phys. Rev. Lett. **92**, 126801 (2004).
[16] J. D. Jackson, *Classical Electrodynamics* (John Wiley & Sons, New York, 1975).
[17] E. V. Tsiper and Z. G. Soos, Phys. Rev. B **68**, 085301 (2003).
[18] A. Toriumi, T. Yokoyama, T. Nishimura, T. Yamada, K. Kita, and K. Kyuno, Proc. Electrochem. Soc. **2004–15**, 237 (2004).
[19] T. Kawatsu, V. Coropceanu, A. Ye, and J.-L. Bredas, J. Phys. Chem. C **112**, 3429 (2008).
[20] H. Ohkita, S. Cook, Y. Astuti, W. Duffy, S. Tierney, W. Zhang, M. Heeney, I. McCulloch, J. Nelson, and D. Bradley *et al.*, J. Am. Chem. Soc. **130**, 3030 (2008).